J Mater Sci (2011) 46:1103–1109
DOI 10.1007/s10853-010-4879-4

Influence of N and Fe on α-Ti precipitation in the in situ TiC–titanium alloy composites

G. Amirthan · K. Nakao · M. Balasubramanian · H. Tsuda · S. Mori

Received: 26 April 2010 / Accepted: 30 August 2010 / Published online: 14 September 2010

Abstract High strength with high ductility can be achieved in the titanium alloys by using metal precipitated ceramic particle as reinforcement. In this work, $\alpha + \beta$ or β-Ti alloy composites were prepared with α-Ti precipitated TiC particles. A series of Ti–Fe–C–N alloys were prepared and a constitutional diagram was constructed as a function of N and Fe contents. Two criteria were identified for the formation of α-Ti precipitation. One is the existence of Ti_2C phase and the other is the presence of α-Ti phase in the matrix. The mechanism of α-Ti formation from the Ti_2C phase is discussed.

Introduction

Titanium alloys are important engineering materials for the fabrication of medical and dental implants due to their attractive properties [1–3]. These include high specific strength, high resistance to corrosion, biocompatibility, and tailorable Young's modulus. Over the past few years, $\alpha + \beta$ and β-titanium alloys have been considered as a very important class of materials because of their high strength, low density, and good corrosion resistance [4–6]. Currently, key components fabricated from β-Ti alloys are found in many fields, like aerospace, biomedical, sports and consumer goods, gas/oil, and naval, etc. Although they have high strength, their ductility is low at room temperature. Attempts have been made to improve the ductility of these alloys by various techniques [6, 7]. Reinforcing the alloy with metal precipitated hard ceramic is more fascinating, since the strength and ductility can be improved simultaneously. It has been reported that the metal-precipitated ceramic particle in the metal matrix is soft in nature and is helping to improve the ductility of the composite [8]. Since the β-Ti alloys have been considered as a potential material for many applications, it will be useful to make a metal precipitated TiC particle reinforced β-Ti composite with better properties. Iron can be used as a β-Ti stabilizing element since it is a cheap and good bio-compatible element [9–11]. The mechanical properties of these composites are very sensitive to the microstructure of the TiC particle. Hence, the present study tries to point out some of the critical microstructural changes in the TiC particles by the combined effect of N and Fe elements. To accomplish this, a series of $\alpha + \beta$ and β-titanium alloy composites were prepared by reactive arc-melting method. The microstructures of TiC particle and Ti matrix were investigated by optical and transmission electron microscopy. X-ray diffraction technique was used to identify the phases.

Experimental procedure

Ti powder (99.9%, 350 mesh), C powder (Graphite, 99.98%, 25 μm), TiN powder (99.5%, 350 mesh), and Fe powder (99 + %, 325 mesh) were used as starting materials. The compositions selected for this study are Ti-(3, 5, 7, 8, 9, or 10) % Fe-4% C-(0, 1, 3, or 5) % N (all in at.%). The required quantities of powders were mixed in the agate mortar and pestle to get homogeneous mixture.

G. Amirthan (✉) · M. Balasubramanian
Department of Metallurgical and Materials Engineering, Indian Institute of Technology Madras, Chennai 600036, India
e-mail: amirthan01@yahoo.com

G. Amirthan · K. Nakao · H. Tsuda · S. Mori
Department of Materials Science, Graduate School of Engineering, Osaka Prefecture University, Osaka 5998531, Japan

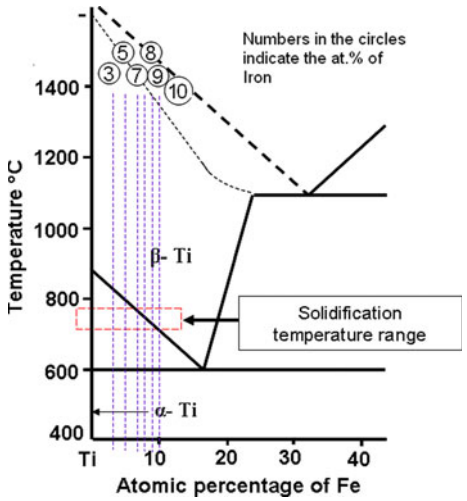

Fig. 1 Ti–Fe phase diagram

Subsequently, these mixtures were uni-axially pressed in a cylindrical die of 10 mm diameter under a pressure of 230 MPa. Then, the 30 g button ingots of alloys were prepared from the above pellets using a non-consumable arc-melting method under Ar atmosphere. The ingots were flipped and re-melted for four times to ensure compositional homogeneity. The expected amount of TiC particles in the composite is 5 vol.% for all the alloys. The alloy compositions chosen for this study are located in the Ti–Fe phase diagram, as shown in Fig. 1 [12]. The X-ray diffraction (XRD) patterns of the alloys were recorded using X-ray diffractometer (Rigaku, Multiflex) with nickel filtered Cu K_α radiation.

For optical microscopy analysis, the samples were prepared according to the standard metallographic procedure. The first step was plane grinding with SiC paper up to 1000 grid. The plane grinding was followed by electropolishing. Electropolishing was carried out using a standard solution (80% Methanol + 20% Nitric acid) by applying 24 V at a temperature of −30 °C. The samples were etched using Kroll's solution after polishing. Specimens were analyzed using an optical microscope (Olympus, BX51M, Japan) and Scanning Electron Microscope (JEOL-JXA-8800) equipped with electron probe mapping analysis.

The samples for TEM examination were first ground with SiC papers up to 2000 grid. The sample thickness after mechanical polishing was maintained below 70 μm. Subsequently, the final specimen thinning was carried out using a twin-jet electropolishing machine (Tenupol-3, Struer) with a solution containing HNO_3 and methanol (20:80) at temperatures between −50 and −40 °C. Transmission electron microscope (JEM-2000FX) operating at 200 kV was used to investigate the microstructure of TiC particle and Ti matrix.

The sample notation is given as XFeYN, where X is Fe content and Y is N content. For example, sample 3Fe0N means 3 at.% Fe and 0 at.% N. Carbon content is fixed at 4 at.% for all the alloys and the remaining metal is Ti.

Results and discussion

XRD patterns of 0N alloy series as a function of iron content are shown in Fig. 2. XRD analysis confirmed the presence of α-Ti, β-Ti, and TiC phases in Ti-(3, 5, 7, 8, 9, 10) % Fe alloys. It clearly shows that the intensity of the α-Ti peaks gradually decreases with increasing Fe content and the peak completely disappeared in the 10Fe system. This indicates that the matrix is gradually becoming β-Ti on increasing the iron content.

XRD patterns of 3Fe alloy series as a function of nitrogen content are shown in Fig. 3. It clearly shows the shift of TiC peaks toward higher angle on increasing the N content. This implies that the composition of the TiC is

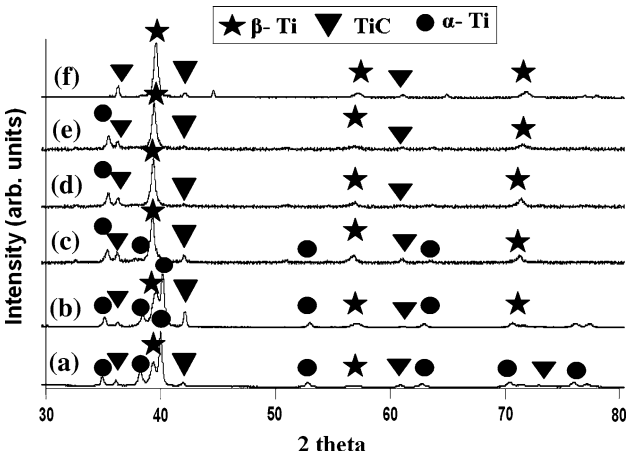

Fig. 2 XRD patterns as a function of Fe (**a**) 3Fe0N, (**b**) 5Fe0N, (**c**) 7Fe0N, (**d**) 8Fe0N, (**e**) 9Fe0N, and (**f**) 10Fe0N

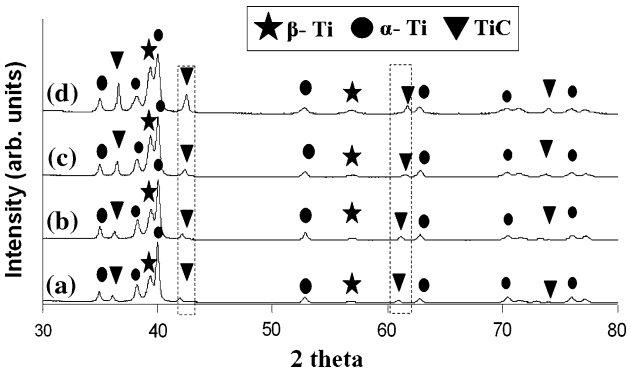

Fig. 3 XRD patterns as a function of N (**a**) 3Fe0N, (**b**) 3Fe1N, (**c**) 3Fe3N, and (**d**) 3Fe5N

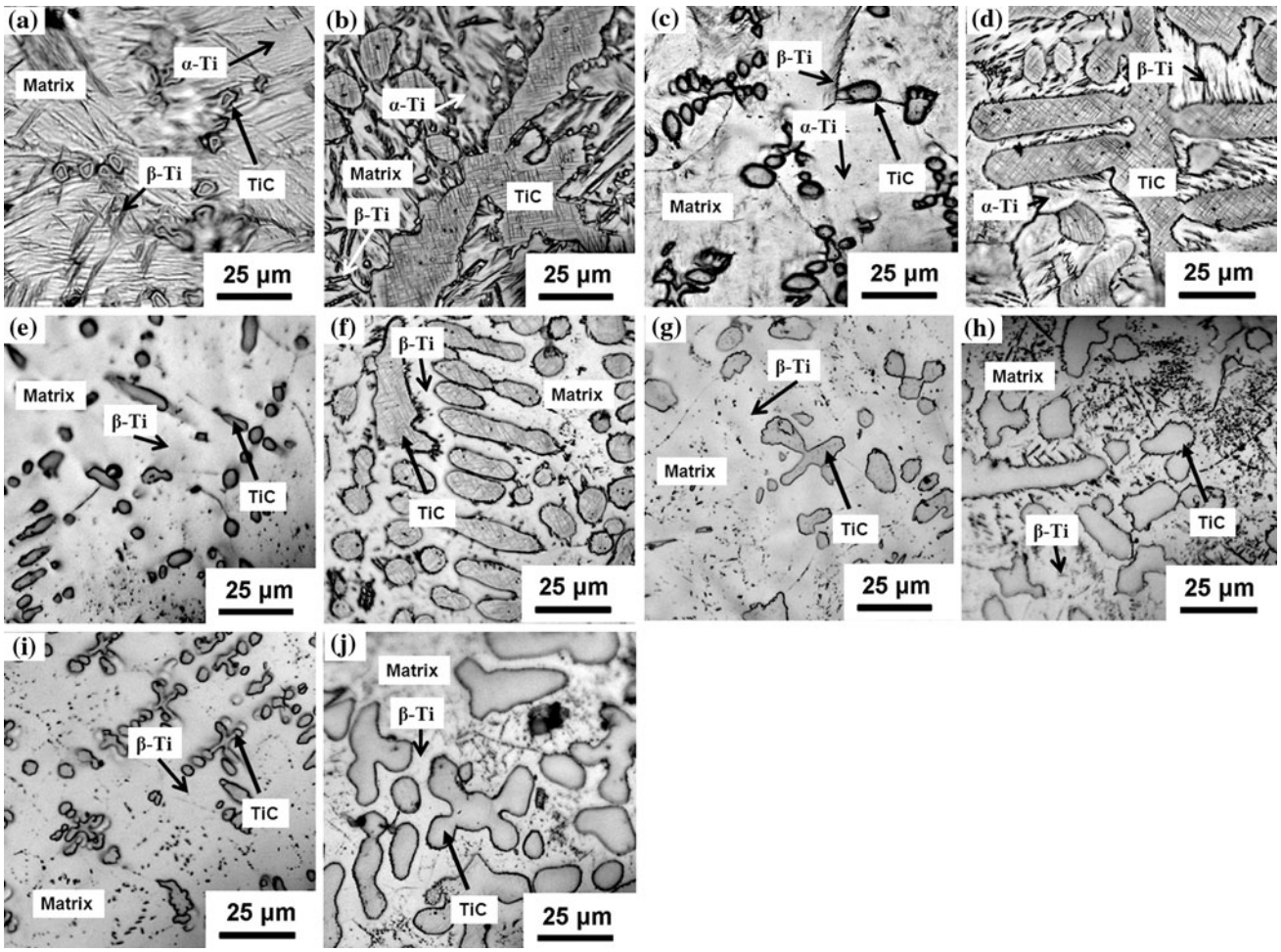

Fig. 4 Optical Micrograph of (**a**) 3Fe0N, (**b**) 3Fe5N, (**c**) 5Fe0N, (**d**) 5Fe5N, (**e**) 7Fe0N, (**f**) 7Fe5N, (**g**) 9Fe0N, (**h**) 9Fe5N, (**i**) 10Fe0N, and (**j**) 10Fe5N

titanium rich and non-stoichiometric nature. On the other hand, the lattice parameters of "*c*" axis of α-Ti and "*a*" axis of *β*-Ti are increasing with increasing nitrogen content. This shows the entry of N atoms into the crystals of α- and *β*-Ti phases. It has been reported that the lattice constant of the TiC crystal structure depends on C/Ti atomic ratio and is gradually decreasing with increasing Ti content [13]. Similarly, Bars et al. [14] observed the lattice constant expansion along the "*a*" and "*c*" axis when the N atoms enter the α-Ti. Hence, this information can be used to explain the lattice parameter changes in TiC and α-Ti. The entry of N atoms into the TiC lattice may also reduce the C/Ti ratio of the TiC phase and hence there is a decrease in the lattice constant of the TiC crystals. On the other hand, the entry of N atoms in the interstitial space in the h.c.p structure of α-Ti leads to the expansion along "*a*" and "*c*" axes.

Optical micrographs of some selective compositions are shown in Fig. 4. These clearly show that the changes in the surface morphology of TiC particles and the matrix are caused by the addition of N and Fe. Also, it can be seen that the size of the TiC particle is highly sensitive to the nitrogen content of the alloy. Moreover, the α and *β* phases seem to coexist (Fig. 4a–d). However, the proportion of the α phase decreases with the increase of iron content and the α phase completely disappears when the Fe content is 9% and above (Fig. 4e–h). On the other hand, in 3Fe0N alloy, the average diameter of TiC particle is less than 15 μm and there is no α-Ti precipitation. When 5% N is added to the above system, the TiC particle size increases up to 60 μm and the surface contains fine platelets of α-Ti. Similar trend is observed in 5Fe alloy series. When the iron content is increased to 7% and above (especially 5% N case), the TiC particles grow as in the 3Fe and 5Fe systems. However, the amount of α-Ti precipitation in the TiC particle is gradually decreased and even completely disappeared when the iron content is 9% and above. Figure 5 shows the SEM micrographs of TiC particle in the 3Fe5N and 10Fe5N

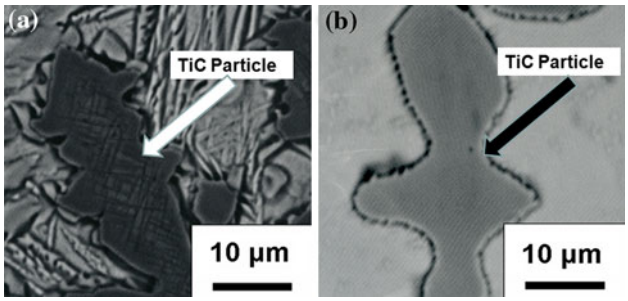

Fig. 5 SEM micrograph of surface morphology of TiC particle at higher magnification (**a**) 3Fe5N and (**b**) 10Fe5N

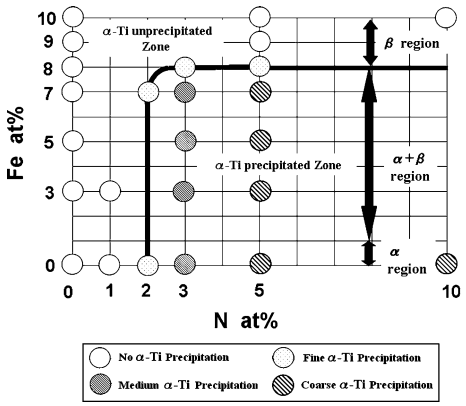

Fig. 6 Constitutional diagram of α-Ti precipitation appearance in the TiC particle as a function of N and Fe at.%

system at a higher magnification. The α-Ti platelets are clearly visible in the 3Fe5N system, whereas in the latter the particle surface is free from the α-Ti platelets. Figure 6 is a constitutional diagram as a function of Fe and N contents. It shows the combination of Fe and N contents at which the α-Ti precipitations in the TiC particles are observed. The open circles in Fig. 6 indicate the alloys where the α-Ti precipitation in the TiC particles is absent. Similarly, closed circles indicate the presence of α-Ti precipitates in the TiC particle. In particular, light and dark shaded closed circles indicate the amount of the α-Ti precipitation in the TiC particle, i.e. the darker the shade, the higher is the amount of α-Ti precipitation in the TiC particle. It can be clearly seen from the Fig. 6 that the α-Ti precipitation is observed only when the nitrogen content is more than 3 at.% and the iron content is less than 8 at.% in the alloys.

TEM micrographs and SAD patterns of 3 Fe alloys and 10 Fe alloys are shown in Fig. 7. In 3Fe0N alloy, there is no evidence of α-Ti precipitation. The SAD pattern shows diffused spots, which may correspond to the Ti_2C phase. It indicates the non-stoichiomertic nature of the TiC particle and the long range order of Ti_2C phase. When the nitrogen content in the above alloy is 3%, fine platelets of α-Ti precipitates started to form and the SAD pattern shows the coexistence of Ti_2C and α-Ti. On further addition of nitrogen (5% and more), coarse α-Ti platelets are more apparent in the micrograph and the diffused Ti_2C spots are completely obscured in the SAD pattern (Fig. 7c, d). The microstructure and SAD pattern of 10Fe0N alloy closely resemble to the 3Fe0N alloy. Interestingly, the TEM micrograph of 10Fe5N alloy shows no evidence of α-Ti precipitation in the TiC particle. The SAD pattern also shows no evidence for the existence of α-Ti precipitate. This is in good agreement with the optical microscopic observation. The crystallographic relationship between the observed Ti_2C, TiC, and the precipitated α-Ti is $(111)\ Ti_2C//(111)TiC//(0001)\ \alpha\text{-Ti}$, $[011]Ti_2C//[011]\ TiC//[2\bar{1}\bar{1}0]\alpha\text{-Ti}$. From the above observation, one can infer that the Ti_2C phase in the TiC particle is playing a vital role in the formation of α-Ti precipitation, however, that depends on the N and Fe content in the alloy.

In general, there are two criteria for the formation of α-Ti precipitation in the TiC particle, i.e. (i) N content and (ii) prevalence of the α-Ti in the matrix. If the N content is less than 2%, there is no α-Ti precipitation in the TiC particle. Similarly, if the matrix contains only β-Ti phase, as in 10Fe5N alloys, it suppresses the formation of α-Ti precipitation in the TiC particle.

Following discussion explains the mechanism of α-Ti precipitation in the TiC particle with the help of crystal structure and phase diagram. In general, titanium carbide crystallizes to the cubic sodium chloride (B1) structure within a broad homogeneity range (TiC_x, $0.48 \leq x \leq 1.0$) with statistically distributed substitutional vacancies on the carbon sublattice sites [15]. Non-stoichiometry is very common in this compound [16]. Its physical properties are significantly influenced by the amount of structural vacancies [17]. Figure 8 shows the crystal structures and corresponding diffraction patterns of TiC and Ti_2C. The space group of the stoichiometric TiC is Fm3m with a lattice parameter of 4.328 Å (Fig. 8a). From TiC_x samples in the composition range $0.5 \leq x \leq 0.7$, two different ordered defect structures of Ti_2C have been recognized experimentally. These include cubic Ti_2C of space group symmetry Fd3m and trigonal Ti_2C of space group $R\bar{3}m$ (Fig. 8b) [18]. Within the $R\bar{3}m$ space group, Ti_2C has two different crystal structures and are shown in Fig. 8b.

Neglecting the trigonal distortion, the two order defect structures have identical atomic distances and atomic pair correlations, and although they differ in their atomic arrangement, they cannot be distinguished by means of X-ray diffraction, electron diffraction, or neutron diffraction [19]. The lattice parameter of cubic Fd3m-Ti_2C (Ti_2C (I)), with experimental value of 8.6 Å, is twice as large as the lattice parameter of the B1 structure (Fig. 9). The

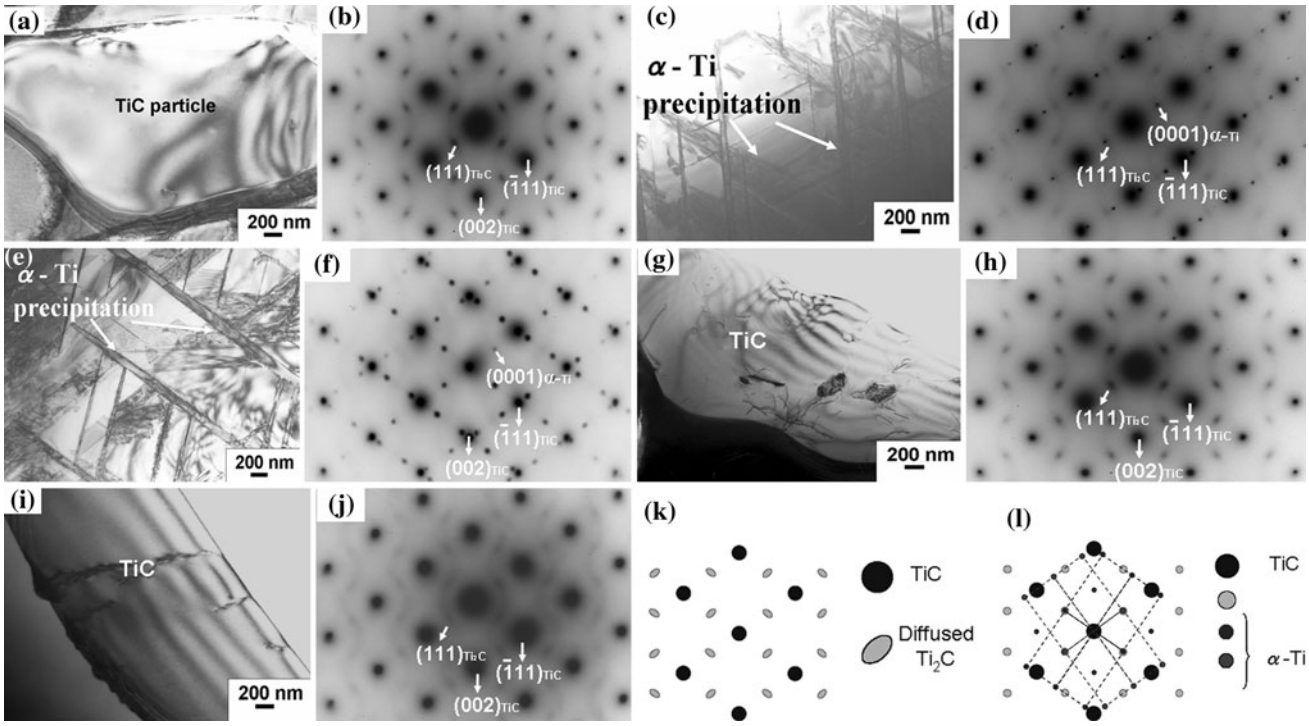

Fig. 7 TEM micrographs and SAD patterns (**a**) and (**b**) 3Fe0N, (**c**) and (**d**) 3Fe3N, (**e**) and (**f**) 3Fe5N, (**g**) and (**h**) 10Fe0N, (**i**) and (**j**) 10 Fe5N, (**k**) and (**l**) key diagram of 3Fe0N and 3Fe5N, respectively. Incident beam is parallel to [011] direction of TiC and $[2\bar{1}\bar{1}0]$ direction of α-Ti

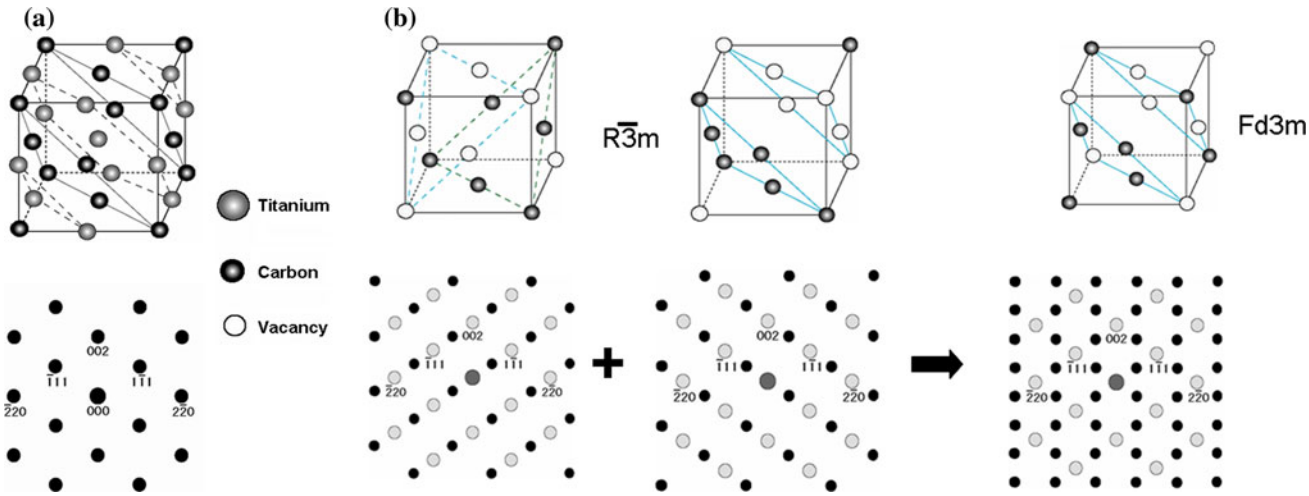

Fig. 8 Crystal structures and corresponding SAD patterns (**a**) TiC (**b**) Ti_2C (Ti plane invisible)

lattice parameter of the one-eighth of the cubic unit cell is 4.3 Å, which is comparable with the lattice parameter of the stoichiometric TiC (4.328 Å). In Fd3m-Ti_2C, the filling of the C (111) planes alternates from 1/4 to 3/4. For R$\bar{3}$m-Ti_2C, the alternating C (111) planes are either fully occupied or completely unoccupied [20].

The SAD pattern of the Fd3m-Ti_2C closely resembles the SAD pattern of 3Fe0N and 10Fe0N. It is very difficult to distinguish the Ti_2C space group just by considering the SAD pattern, since the above two R$\bar{3}$m crystal structures combine to form a SAD pattern that is much similar to the Fd3m if they are finely distributed within the TiC particle (Fig. 8). However, the Fd3m structure is considered to explain the α-Ti precipitation formation mechanism. Figure 10 shows the Ti_2C (Fd3m) atomic planes in the [111] direction. The Ti atomic plan stacking sequence in this structure is ABCABC. The calculated distance between the A–C plane is 4.97 Å. On the other

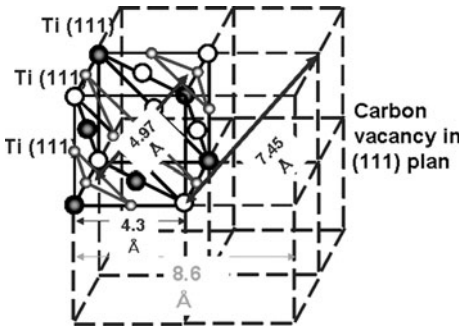

Fig. 9 Unit cell of the Ti_2C-Fd3m crystal structure

hand, the Ti atomic plan staking sequence in the α-Ti hexagonal structure is ABAB, the distance between the A–A plane is 4.77 Å. Let us assume that the one-eighth of the Ti_2C cubic (Fd3m) unit cell co-exists with the α-Ti hexagonal structure as shown in Fig. 11, where the Ti (111) plane in the Ti_2C is parallel to the α-Ti (0001) plan as indicated by the TEM observation. If nitrogen is added, the Ti_2C lattice constant starts to decrease, because of the contraction of the TiC lattice parameter when it is deviated from the stoichiometric nature. Moreover, both TiN and TiC have the NaCl structure, formed by two fcc sublattices, where the Ti atoms occupy one sublattice and the carbons and nitrogens occupy the other [21, 22]. It is usually assumed that the vacancy sites are statistically distributed over the non-metallic atom sublattice [18]. These two compounds usually form an isomorphous phase diagram, where the lattice parameter of the stoichiometric TiC ($a = 4.327$ Å) is larger than those of stoichiometric TiN ($a = 4.241$ Å), and the lattice parameter of the TiC decreases with the increasing nitrogen concentration. On the other hand, the α-Ti lattice constant, especially the c axis increases with increasing nitrogen amount. It is known that the nitrogen atoms stay in interstitial sites. In the hexagonal structure, there are octahedral and tetrahedral sites, the latter being smaller than the former. Therefore, one usually assumes that the nitrogen atoms preferentially occupy the octahedral sites. The c parameter is increased more than the a parameter, which corresponds to the expansion of the lattice in the <0001> direction [23]. As stated earlier, Bars et al. [14] showed that the c parameter increases quickly for concentrations up to 10 at.% N and more slowly for concentrations between 10 and 22 at.% N. However, in all cases, the hexagonal lattice deformation is more important in the <0001> direction.

From the above explanations, it is possible to propose the formation mechanism for α-Ti phase from the Ti_2C phase. Nitrogen atoms present in the Ti_2C structure build-up strains which induce a deformation of the cubic lattice by decreasing the "a" parameters without changing the lattice symmetry due to the atomic size difference of the carbon and nitrogen atoms, whose sizes are 1.6 and 1.5 Å, respectively. Hence, the interplanar distance of Ti (111) planes is gradually reduced and approaching the interplanar distance of α-Ti (0001) planes (Fig. 11). This structure remains stable until nitrogen reaches the certain solubility limit and in the present case, it is 2%. On further addition of nitrogen (3% and above), certain regions become unstable and their structure changes to the hexagonal structure of α-Ti. From a crystallographic point of view, the transformation of Ti_2C into α-Ti may be visualized by the sliding of a (111) plane of the cubic structure which becomes a (0001) plane of the hexagonal structure, since the difference between both structures is only in the stacking sequences which are of the ABCABC type in the first case and the ABABAB type in the second [24].

Besides the nitrogen content, Fe content also has an effect on the α-Ti formation, when it is 9% and above. This can be explained with a help of Ti–Fe phase diagram,

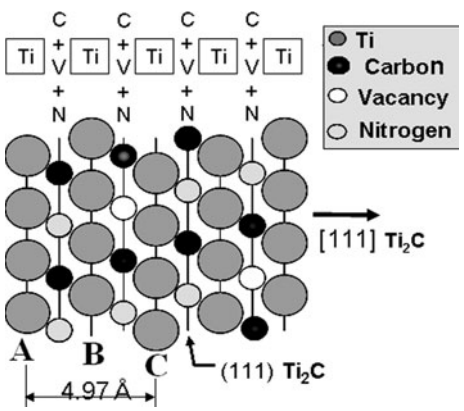

Fig. 10 Atomic planes along [111] direction in Ti_2C-Fd3m structure

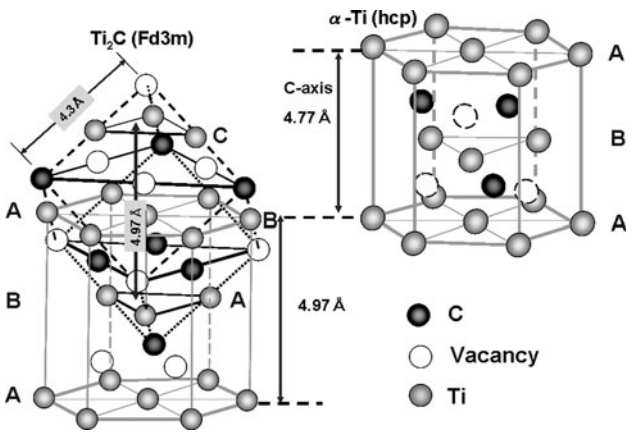

Fig. 11 Schematic diagram of co-existence of Ti_2C-Fd3m crystal structure with α-Ti hexagonal crystal structure

shown in Fig. 1. As can be seen from the figure, when the alloys with high iron content are cooled from the β phase region, β is the only equilibrium phase. Therefore, it may restrain the formation of α-Ti precipitate in the TiC particle.

Conclusion

TiC particle reinforced $\alpha + \beta$ or β-Ti alloy composites were prepared by reactive arc-melting method. The α-Ti precipitation is observed in the TiC particles only when the nitrogen content is more than 3 at.% and the iron content is less than 8 at.%. Existence of the Ti_2C phase in the TiC particle is a prerequisite for the formation of α-Ti precipitation in the TiC particles, which in turn depends on the Fe content. The crystallographic relationship between the TiC, Ti_2C, and precipitated α-Ti can be described by:

$$(111)\ Ti_2C//(111)\ TiC//(0001)\ \alpha\text{-Ti},$$
$$[011]\ Ti_2C//[011]\ TiC//[2\bar{1}\bar{1}0]\ \alpha\text{-Ti}$$

Acknowledgement This work was supported by a Grant in aid for Scientific Research (c) from the Ministry of Education, Culture, Sports, Science and Technology, Japan.

References

1. Boyer RR (1993) In: Eylon D, Boyer RR, Koss DA (eds) Beta titanium alloys in the 1990s. TMS, Warrendale, PA
2. Andoa T, Nakashima K, Tsuchiyama T, Takaki S (2008) Mater Sci Eng A 486:228
3. Mantani Y, Tajima M (2006) Mater Sci Eng A 442:409
4. Lutjering G (1998) Mater Sci Eng A 243:32
5. Das J, Tang MB, Kim KB, Theissmann R, Baier F, Wang WH, Eckert J (2005) Phys Rev Lett 94:205
6. Hays CC, Kim CP, Johnson WL (2000) Phys Rev Lett 84:2901
7. Furuhara T, Ogawa T, Maki T (1995) Philos Mag 72:175
8. Tsuda H, Mori H, Mastui T, Mabuchi H, Morii K (2006) In: 16th international microscopy congress, Sapporo, Japan
9. Das J, Kim KB, Baier F, Loser W, Gebert A, Eckert J (2007) J Alloys Compd 434:28
10. Bhattacharyya D, Viswanathan GB, Denkenberger R, Furrer D, Fraser HL (2003) Acta Metall 51:4679
11. Kuroda D, Kawasaki H, Yamamoto A, Hiromoto S, Hanawa T (2005) Mater Sci Eng C25:312
12. Okamoto H (1996) J Phase Equilib 17:369
13. Storms EK (1967) In: The refractory carbides, vol 2. Academic Press, London
14. Bars JP (1983) Metall Mater Trans A 14:1537
15. Eibler R (2002) J Phys Condens Matter 14:4425
16. Quinn CJ, Kohlstedt DL (1984) J Am Ceram Soc 67:305
17. Eibler R (2007) J Phys Condens Matter 19:196
18. Wriedt HA, Murray JL (1987) Bull Alloy Phase Diagr 8:378
19. Poulek V, Musil J, Valvoda V, Cerny R (1988) J Phys D Appl Phys 21:1657
20. Han K, Weatherly GC (1997) Philos Mag 76:247
21. Lipatnikov VN, Kottar A, Zueva LV, Gusev AI (2000) Inorg Mater 36:155
22. Gusev AI, Rempel AA (1997) Phys Status Solidi A 163:273
23. Gusev AI (1989) Philos Mag B 60:307
24. Guemmaz M, Mosser A (1997) Appl Phys A 64:407